Published in final edited form as:
Cancer Discov. 2014 August ; 4(8): 896–904. doi:10.1158/2159-8290.CD-13-0230.

Vulnerabilities of PTEN-p53-deficient prostate cancers to compound PARP/PI3K inhibition

Enrique González-Billalabeitia[1,2,*], **Nina Seitzer**[1,*], **Su Jung Song**[1], **Min Sup Song**[1], **Akash Patnaik**[3,4,5], **Xue-Song Liu**[1], **Mirjam T. Epping**[1], **Antonella Papa**[1], **Robin M. Hobbs**[1], **Ming Chen**[1], **Andrea Lunardi**[1], **Christopher Ng**[1], **Kaitlyn A. Webster**[1], **Sabina Signoretti**[7,8], **Massimo Loda**[7,8,9,10], **John M. Asara**[4], **Caterina Nardella**[1,6], **John G. Clohessy**[1,6], **Lewis C. Cantley**[4,5], and **Pier Paolo Pandolfi**[1]

[1]Cancer Genetics Program, Beth Israel Deaconess Cancer Center, Department of Medicine, Beth Israel Deaconess Medical Center, Harvard Medical School, Boston MA 02115, USA

[2]In leave of absence: Servicio de Hematología y Oncología Médica. Hospital Universitario Morales Meseguer, Murcia. Spain

[3]Division of Hematology/Oncology, Department of Medicine, Beth Israel Deaconess Medical Center, Harvard Medical School, Boston, MA 02115, USA

[4]Department of Systems Biology, Harvard Medical School, Boston, MA 02115, USA

[5]Division of Signal Transduction, Department of Medicine, Beth Israel Deaconess Medical Center, Harvard Medical School, Boston MA 02115

[6]Preclinical Murine Pharmacogenetics Facility, Beth Israel Deaconess Medical Center, Harvard Medical School, Boston, MA 02115, USA

[7]Center for Molecular Oncologic Pathology, Dana-Farber Cancer Institute, Boston, MA 02115, USA

[8]Department of Medical Oncology, Dana-Farber Cancer Institute, Boston, MA 02115, USA

[9]Department of Pathology, Brigham and Women's Hospital, Harvard Medical School, Boston, MA 02115, USA

[10]Broad Institute of Harvard and Massachusetts Institute of Technology, Cambridge, MA 02215, USA

Abstract

Corresponding Author: Pier Paolo Pandolfi, Cancer Genetics Program, Beth Israel Deaconess Cancer Center, Department of Medicine, Beth Israel Deaconess Medical Center, Harvard Medical School, Boston MA 02115, USA, Phone:617-735-2121, Fax: 617-735-2120, ppandolf@bidmc.harvard.edu.
*These authors contributed equally to this work

The authors disclose no potential conflicts of interest.

Author Contributions

P.P.P. supervised the project; E.G., N.S., S.J.S., M.S.S., C.N., J.C., L.C. and P.P.P. designed experiments; E.G., N.S., S.J.S., M.S.S., A.P., X.S.L., A.P., J.M.A, A.L., M.C., R.H., C.N., K.A.W. and M.E. performed experiments; M.L. and S.S. reviewed all mouse pathology; E.G., N.S., S.J.S., M.S.S., J.C., C.N., L.C. and P.P.P. critically discussed the results and the manuscript; E.G., N.S., S.J.S, M.S.S., J.C. and P.P.P. analysed the data and wrote the paper.

Prostate cancer (CaP) is the most prevalent cancer in males and treatment options are limited for advanced forms of the disease. Loss of the PTEN and p53 tumor suppressor genes is commonly observed in CaP, while their compound loss is often observed in advanced CaP. Here we show, that PARP inhibition triggers a p53-dependent cellular senescence in a *PTEN*-deficient setting in the prostate. Surprisingly, we also find that PARP-induced cellular senescence is morphed into an apoptotic response upon compound loss of PTEN and p53. We further show that superactivation of the pro-survival signalling PI3K-AKT pathway limits the efficacy of a PARP-single-agent treatment, and that PARP and PI3K inhibitors effectively synergize to suppress tumorigenesis in human CaP cell lines and in a *Pten/p53* deficient mouse model of advanced CaP. Our findings therefore identify a combinatorial treatment with PARP and PI3K inhibitors as an effective option for *PTEN*-deficient CaP.

Keywords

PTEN; Prostate; PARP; PI3K; Senescence

Introduction

There is an urgent need for the development of novel successful strategies for advanced CaP in order to improve patient outcomes (1,2).

The loss of at least one allele of *P*hosphatase and *ten*sin homolog deleted on chromosome 10 (*PTEN*) is observed in more than 40% of prostate cancers (3,4). As a lipid phosphatase, PTEN suppresses the activation of the phosphoinositide 3-kinase (PI3K)-AKT signaling cascade that is a central proto-oncogenic signalling hub in prostate cancer development (5–9). Notably, PTEN also exerts tumor suppressive functions in the nucleus by regulating genomic instability, and DNA repair defects driven by *PTEN*-loss have been proposed as a rationale for the sensitivity to Poly-(ADP ribose) protein (PARP) inhibitors comparable to the enhanced sensitivity of BRCA-deficient cancers (5,10–12). On this basis, we therefore aimed to test whether PARP inhibition, singly or when combined with PI3K inhibition, would represent effective therapeutic modalities in prostate cancer.

Results

Common genetic alterations in prostate cancer morph senescence into apoptosis in response to PARP inhibition

We first aimed to determine whether common genetic alterations in prostate cancer respond towards Olaparib. To mimic different stages of prostate cancer progression we selected $Pten^{+/-}$, (early stage), $Pten^{Lx/Lx}$ (advanced hormone sensitive) and $Pten^{Lx/Lx};Trp53^{Lx/Lx}$ MEFs (advanced hormone insensitive) (Figure S1A) to perform a cell proliferation assay upon treatment with 10uM Olaparib. Interestingly, MEFs of all genotypes (Figure 1A–C) showed a significant growth inhibition upon exposure to Olaparib. Surprisingly, in contrast to $Pten^{Lx/Lx};Trp53^{Lx/Lx}$ MEFs, $Pten^{+/-}$ and $Pten^{Lx/Lx}$ MEFs showed a robust senescence response (Figure S1B and S1C), that was significant and dose dependent in $Pten^{+/-}$ (Figure 1D) as well as $Pten^{Lx/Lx}$ (Figure 1E) compared to wt MEFs. Strikingly and surprisingly,

further analysis revealed that in contrast to *Pten*$^{Lx/Lx}$ MEFs, *Pten*$^{Lx/Lx}$*;Trp53*$^{Lx/Lx}$ MEFs showed a significant increase in apoptosis rather than senescence (Figure S1C and 1F) as analysed by Annexin V staining (Figure S1D and S1E) and detection of cleaved Caspase 3/7 (Figure 1G).

Western Blot analysis of *Pten*$^{Lx/Lx}$ and *Pten*$^{Lx/Lx}$*;Trp53*$^{Lx/Lx}$ MEFs treated with increasing concentrations of Olaparib revealed that whereas *Pten*$^{Lx/Lx}$ MEFs showed a further increase in p53 protein levels, both *Pten*$^{Lx/Lx}$ *and Pten*$^{Lx/Lx}$*;Trp53*$^{Lx/Lx}$ MEFs showed increased DNA-damage as visualized by γH2AX staining (Figure 1H). This analysis demonstrates that the senescence response in *Pten*$^{Lx/Lx}$ is likely driven by the induction of p53 as previously described (13). However, the concomitant loss of p53 induces increased DNA damage that in turn morphs this phenotype into an apoptotic response.

PARP inhibition induces a differential response *in vivo* with a modest effect on overall tumor response

In order to validate our findings *in vivo*, we next studied the sensitivity of Genetically Engineered Mouse Models (GEMMs) of CaP towards PARP inhibition. Similar to our *in vitro* analysis, we enrolled *Pten*$^{+/-}$, *Pten*$^{Lx/Lx}$*;Probasin-Cre* (referred to as *Pten*$^{pc-/-}$) and *Pten*$^{Lx/Lx}$*;Trp53*$^{Lx/Lx}$ *Probasin-Cre* (referred to as *Pten*$^{pc-/-}$*;Trp53*$^{pc-/-}$*)* mice. In line with the data observed in MEFs, pharmacological inhibition of PARP induced a strong and significant induction of senescence in *Pten*$^{+/-}$ (Figure S2A) and *Pten*$^{pc-/-}$ (Figure 2A and B) models compared to vehicle treated controls. In *Pten*$^{pc-/-}$ mice the senescence response was accompanied by an increased DNA damage as analysed by γH2AX of treated prostate tumors (Figure S2B). Histological analysis of *Pten*$^{pc-/-}$ tumors treated with Olaparib revealed a modest decrease of high-grade prostatic intraepithelial neoplasia (HGPIN) (Figure 2C). However, this trend did not reach statistical significance.

Next we tested whether *Pten*$^{pc-/-}$*;Trp53*$^{pc-/-}$ mice show a similar apoptotic response upon treatment with Olaparib as observed *in vitro*. In line with the *in vitro* data, Olaparib treatment increased γH2AX in DLP tumors of *Pten*$^{pc-/-}$*;Trp53*$^{pc-/-}$ mice (Figure S2C). Surprisingly, macroscopic analysis and cytokeratin 8 staining (luminal cells) of Olaparib-treated prostates revealed that more glands were lined by a single-layer compared to vehicle control (Figure 2D and S3A). Additionally, analysis of cytokeratin 14 showed a reduction of the intermediate basal cell population in single-layered glands suggesting a certain degree of normalization after treatment (Figure S3B). TUNEL and Caspase-3 staining further revealed a significant increase in apoptotic cells upon Olaparib treatment (Figure 2E, 2F, S2D). However, similar to *Pten*$^{pc-/-}$ mice, histological analysis of *Pten*$^{pc-/-}$*;Trp53*$^{pc-/-}$ tumor reduction after drug treatment did not reach statistical significance (Figure 2G) suggesting that single-agent Olaparib treatment is not sufficient to induce a robust anti-tumor response in these models. Interestingly, mass spectrometry analysis of Olaparib in prostates revealed that only ~2uM of the drug is delivered into the individual lobes, an amount that is significantly lower when compared to the dose utilized in our *in vitro* studies (Figure S3C). This marked difference in drug concentration may in turn provide one possible explanation for the limited overall tumor response *in vivo*.

Hyperactivation of the PI3K-Akt pathway impacts sensitivity towards Olaparib

Based on our data in mice we sought to determine whether Olaparib could trigger a similar response in human prostate cancer cell lines. To this end, we engineered LnCap cells that lack Pten to additionally loose p53 function by either overexpressing a p53 short hairpin construct (Figure S4A) or dominant-negative p53 (p53-DN; Figure S4B). Similar to MEFs, Olaparib induced senescence in a p53-proficient setting that was blunted upon loss of p53 (Figure 3A). In contrast, LnCap cells expressing p53-DN did not show differential sensitivity to Olaparib treatment. Furthermore, only high Olaparib concentrations (10uM) induced a strong growth inhibition overall (Figure 3B) suggesting mechanisms limiting Olaparib efficacy beyond the limited uptake observed *in vivo*.

We therefore investigated whether classical survival signalling such as the PI3K-Akt pathway might be super-activated upon Olaparib exposure and therefore analysed Akt activation upon Olaparib treatment *in vitro* (7,14–16). Indeed, $Pten^{Lx/Lx};Trp53^{Lx/Lx}$ MEFs (Figure 3C) and LnCap cells (Figure 3D) hyperactivated Akt upon exposure to Olaparib, suggesting that Akt could impact the response to Olaparib. Indeed, knockdown of Akt1, the major Akt isoform, significantly increased growth inhibition upon PARP inhibition (Figure S4C and 3E) and induced apoptosis as shown by increased PARP cleavage (Figure 3F).

To investigate the mechanism of Akt hyperactivation, we made use of the dual PI3K inhibitor BKM-120 that efficiently blocked Akt activation in LnCap cells (Figure 3F). Strikingly, PI3K inhibition was able to restore pAkt to DMSO control levels in Olaparib treated cells suggesting that the major activator of Akt upon PARP inhibition is indeed PI3K (Figure 3G). Importantly, analysis of cleaved PARP demonstrated that the combination of PARP and PI3K inhibition shows synergistic apoptosis induction suggesting efficacy for a combinatorial treatment strategy in CaP (Figure 3G).

Combination of PARP and PI3K inhibitors as a novel therapeutic approach

Based on our findings, we next aimed to investigate whether a combination treatment including PARP and PI3K inhibition would be synergistic *in vitro*. To this end, we treated $Pten^{Lx/Lx};Trp53^{Lx/Lx}$ MEFs and human CaP cancer cells with either single or combination therapy (Figure S4D, S4E, S4F and S4G). Indeed, the combination significantly increased growth suppression compared to the single treatments in all tested cell lines.

These promising *in vitro* data prompted us to next evaluate the efficacy of the combinatorial inhibition of PARP and PI3K in our $Pten^{pc-/-};Trp53^{pc-/-}$ model of highly aggressive prostate cancer (Figure S5A). *In vivo* efficacy of control, single agent and the combination arm was assessed by MRI analysis for the dorsolateral prostate (DLP) and the anterior prostate (AP) (Figure S5B and S5C), followed by the analysis of survival and histopathological differences.

To assess the efficacy of PARP and PI3K inhibition *in vivo*, we first followed tumor progression by MRI (Figure 4A). Interestingly, the treatment with Olaparib or BKM120 showed tumor stabilisation but eventually regrew due to potential resistance mechanisms. Strikingly, the combination of the two compounds potentiated tumor stabilisation and induced robust tumor regression. These data indicate that the combinatorial treatment of

PI3K and PARP inhibition is synergistic to the single compound arms *in vivo*. In contrast to the DLP, only slight growth suppression was seen in APs that was potentiated in the combination suggesting a similar cooperation as seen in the DLP albeit with a much lower efficacy (Figure S6A).

We further analysed tumor specimens of all treatment arms after 1–4 weeks by histopathology (Figure 4B,C, S6B and C). Surprisingly, in spite of the initial response towards Olaparib observed at one week, histopathological analysis and cytokeratin 8 staining reveal no difference in the occurrence of HGPIN after 4 weeks compared to the vehicle control. In contrast, the BKM120 treatment arm triggered a clear decrease in HGPIN. Importantly, the combinatorial treatment significantly potentiated this effect, clearly showing cooperation between the two compounds. Furthermore, Cytokeratin 14 staining in the DLPs treated with the combination showed a clear reduction in the intermediate basal cell population that is not apparent in the vehicle or single arm treated tumors. These data indicate a trend towards normalization of the glands specifically in the combination treatment.

In line with this data, progression free survival was markedly improved in the combinatorial treatment arm compared to the single and control arms (Figure 4D S7A and S7B). However and coherently with the lack of response in the AP, overall survival analysis did not reveal a striking difference between the single and combination treatment arms (Figure S7C).

Finally to determine whether the data obtained in our GEMMs could be confirmed in human cell lines we performed xenograft studies using PC3 prostate cancer cell lines (Figure 4E). Similar to our GEMMs, PC3 xenografts displayed a significant and synergistic response when treated with the combination compared to the single agents. Collectively, these data strongly support the notion of a marked cooperative effect between the two drugs for the treatment of CaP.

Discussion

This study allowed us to reach a number of important conclusions:

First, we demonstrate, *in vitro* as well as *in vivo*, that *PTEN* deficiency triggers sensitivity towards PARP inhibition with differential responses. In a p53 proficient setting, loss of *PTEN* triggers a senescence response upon PARP inhibition that is morphed into apoptosis upon loss of p53.

Second, a robust response towards PARP inhibition was only observed at very high concentrations of Olaparib in cell lines, while mouse DLPs treated with Olaparib displayed no significant difference in HGPIN grades. In line with these observations we find that Olaparib only reaches suboptimal concentration *in vivo* in the prostate.

Third, we find that Olaparib, triggers the activation of AKT, a classical cell survival mechanism in response to cellular stresses (7,14–16). These data demonstrated that Olaparib treatment on its own is insufficient to trigger a significant tumor response in the prostate due to a number of reasons.

Fourth, we show that PI3K inhibition by BKM-120 significantly increased sensitivity towards Olaparib both in GEMMs and xenograft models. Importantly, PC3 xenografts showed a clear synergistic effect of growth inhibition in the combination arm *in vivo* validating the efficacy of the combination in a human setting. Intriguingly, these data, especially on PC3, are in clear contrast to the *in vitro* data that rather suggested an additive effect of the combination. These results could be explained by the profound differences in nutrients and growth factors in the two experimental settings, or by the fact that the tumor microenvironment/metabolism may also impact the efficacy of the treatments as previously suggested (17–19).

Lastly, despite these striking findings, combinatorial PARP and PI3K inhibition only prolonged progression-free and overall survival significantly when compared to vehicle, but not to single agent treated animals. However, these data are potentially influenced by the general characteristics of $Pten^{pc-/-};Trp53^{pc-/-}$ prostate tumors (13). Cancers in the APs in this model are intrinsically resistant to therapy including androgen deprivation and only showed a slight growth inhibition in all of the treatment arms (20). However, the rapid growth of the APs strongly influences the survival of $Pten^{pc};Trp53^{pc-/-}$ mice and thus strongly impacts the assessment and interpretation of overall survival.

In conclusion, we show that *PTEN*-deficient CaP is sensitive to PARP inhibition. Due to AKT hyperactivation, and poor pharmacokinetics the *in vivo* efficacy of Olaparib is modest, but concomitant suppression of PARP and PI3K results in a cooperative anti-tumor effect. Thus, the combination of PI3K and PARP inhibitors represents a promising therapeutic approach for the treatment of *PTEN*-deficient prostate tumors.

Methods

Cells

$Pten^{+/-}$, $Pten^{Lx/Lx}$ and $Pten^{Lx/Lx};Trp53^{Lx/Lx}$ MEFs were prepared as previously described. For the excision of target genes, MEFs were retroviral infected with pMSCV-Cre-PURO-IRES-GFP (13).

Human cell lines were obtained from ATCC and cultured according to manufacture's instructions. Cell lines were tested for mycoplasma (MycoAlert, Lonza), but not further authenticated.

Cell proliferation, senescence and apoptosis assays

To study proliferation, cells were plated in a 12-well plate (MEFs at 1.7×10^4 cells/well, prostate cancer cells at 1×10^5 cells/well). After 2–9 days, cells were washed with PBS, fixed with 10% Paraformaldehyde and stained with crystal violet. Crystal Violet was extracted with 10% Acetic Acid and absorbance was detected at 595nm.

To determine senescence, cells were plated in a six-well plate (MEFs at 3.4×10^4 cells/well, LnCap at 1.7×10^4 cells/well). SA-β-Gal was detected after 4 days with the senescence detection kit (Calbiochem) following manufacture's instructions. For quantification more than 200 cells per sample were counted.

For prostate tissue, frozen sections (6 mm) were stained for SA-β-Gal (Calbiochem) following manufacture's instructions. For quantification, slides were digitalized and analyzed with the Aperio Spectrum ImageScope software.

Apoptosis was determined by the Apo-ONE caspase 3/7 assay (Promega) and additionally analysed by a dual Annexin V-APC/7-AAD (BD Biosciences) staining using flow cytometry following manufacturer's instructions.

For *in vivo* apoptosis, samples were analysed with the *in situ* Cell Death Detection Kit (Roche) following manufacture's instructions. For quantification of positive TUNEL staining a total of 500 cells were counted from five different fields.

Western blot and Immunohistochemistry

For western blotting, cell lysates were prepared with RIPA buffer or NP40 Buffer (Boston Bioproducts) supplemented with protease (Roche) and HALT phosphatase inhibitor cocktail (Thermo Scientific) and subsequently subjected to SDS-Gel separation (Invitrogen) and western blotting. The following antibodies were used from Cell signalling: anti-γH2AX, anti-AKT1, anti-mouse Pten, anti-mouse P53, anti-AKT, anti-phospho threonine 308 and anti-phospho-serine 473anti-anti-PARP, anti-cleaved-PARP or human P53 (DO1-Santa Cruz), anti-PAR (BD bioscience), and anti-β-Actin (AC-74; Sigma). Western blots were quantified using Image J software.

For immunohistochemistry (IHC), tissues were fixed in 4% Paraformaldehyde and embedded in paraffin in accordance with standard procedures. H&E staining of sections was performed by the Histology Core at BIDMC.

Drugs

For *in vitro* studies, drugs were resuspended in DMSO (Olaparib, LC Laboratories, 10^{-2}M) (BKM-120, Novartis Pharma AG, 10^{-2}M). For *in vivo* studies, Olaparib in DMSO (50 mg/ml) was diluted in vehicle solution (10% 2-hydroxylpropyl-βCyclodextrine (Sigma)/PB, 10μL/g body) and administered daily by i.p. injection at a dose of 50mg/kg. BKM120 was resuspended in methylcelullose solution at a final concentration of 6 mg/ml and administered daily at a dose of 30 mg/kg by oral gavage.

Mice, xenografts and *in vivo* drug treatments

All mice were maintained in the animal facilities of BIDMC/Harvard Medical School in accordance with institutional rules and ethical guidelines for experimental animal care. All animal experiments were approved by the BIDMC IACUC protocol 066–2011(8,13,21).

For drug treatments, $Pten^{+/-}$ (30 weeks old) and $Pten^{pc-/-}$ (10 weeks old) mice were treated with Olaparib over 2 weeks. $Pten^{pc-/-};Trp53^{pc-/-}$ (4 month old) mice were treated with Olaparib over 1 week.

For the combination treatment of Olaparib and BKM-120, $Pten^{pc-/-};Trp53^{pc-/-}$ (4 month old) mice were evaluated by MRI for the presence of prostate tumours and subsequently enrolled in the following treatment arms: Vehicle, Olaparib, BKM120 or combination at the

same doses. Mice were imaged with MRI before treatment, monitored by MRI until tumor progression and followed for survival analysis. Tumor progression was defined as an increase >50% in tumor volume.

Xenografts were performed with PC3 cells. 1×10^6 cells were injected subcutaneously in the flanks Ncr nude mice (Taconic). Mice were enrolled at a tumor size of $300m^3$ in the following treatment arms: Vehicle, Olaparib, BKM-120, or combination at the same doses. Mice were euthanized after 2 weeks of treatment and tumors subjected to further analysis.

MRI analysis

Mouse prostate images were acquired on an ASPECT Model M2 1T tabletop MRI scanner (ASPECT Magnet Technologies Ltd., Netanya, Israel) and imaged as previously described (20). Tumour volume quantification was performed as previously described (22).

Statistics and Histological analysis

For all statistical analyses GraphPad Prism 6 software was used, and values of $p < 0.05$ were considered statistically significant. Survival was determined by Kaplan Meyer curves. The Mantel-Cox test was used to determine significance between survival curves. All other statistical analysis was done by an unpaired student's t-test.

Scoring of HGPIN status was performed as previously described (23). At least three samples were analysed at the according time points. For the preclinical assessment of the combinatorial treatment in $Pten^{pc-/-};Trp53^{pc-/-}$ mice at least three mice were analysed after 4 weeks of treatment except the vehicle control, where mice were pooled from 1 and 4 week treatment.

Supplementary Material

Refer to Web version on PubMed Central for supplementary material.

Acknowledgments

We would like to thank current members of the Pandolfi lab for critical discussion and Thomas Garvey for insightful editing. We thank Min Yuan and Susanne Breitkopf for help with mass spectrometry experiments and grants NIH 5P01CA120964-04 and NIH DF/HCC Cancer Center Support Grant 5P30CA006516-46 (J.M.A.). E.G. has been supported by a *Bolsa de ampliación de estudios (BAE)* from the *Instituto de Salud Carlos III* (Spain). This work has been supported through the MMHCC/NCI grant (RC2 CA147940-01), R01 GM41890 and P01 CA089021 to P.P.P. and L.C.

References

1. Walsh PC, DeWeese TL, Eisenberger MA. Clinical practice. Localized prostate cancer. N Engl J Med. 2007; 357:2696–705. [PubMed: 18160689]
2. Carter HB, Kettermann A, Warlick C, Metter EJ, Landis P, Walsh PC, et al. Expectant Management of Prostate Cancer With Curative Intent: An Update of The Johns Hopkins Experience. The Journal of Urology. 2007; 178:2359–65. [PubMed: 17936806]
3. Li J. PTEN, a Putative Protein Tyrosine Phosphatase Gene Mutated in Human Brain, Breast, and Prostate Cancer. Science. 1997; 275:1943–7. [PubMed: 9072974]

4. Steck PA, Pershouse MA, Jasser SA, Yung WK, Lin H, Ligon AH, et al. Identification of a candidate tumour suppressor gene, MMAC1, at chromosome 10q23.3 that is mutated in multiple advanced cancers. Nature genetics. 1997; 15:356–62. [PubMed: 9090379]
5. Song MS, Salmena L, Pandolfi PP. The functions and regulation of the PTEN tumour suppressor. Nature Reviews Molecular Cell Biology. Nature Publishing Group. 2012; 13:283–96.
6. Engelman JA, Luo J, Cantley LC. The evolution of phosphatidylinositol 3-kinases as regulators of growth and metabolism. Nature Reviews Genetics. 2006; 7:606–19.
7. Manning BD, Cantley LC. AKT/PKB Signaling: Navigating Downstream. Cell. 2007; 129:1261–74. [PubMed: 17604717]
8. Di Cristofano A, Pesce B, Cordon-Cardo C, Pandolfi PP. Pten is essential for embryonic development and tumour suppression. Nature genetics. 1998; 19:348–55. [PubMed: 9697695]
9. Wu X, Senechal K, Neshat MS, Whang YE, Sawyers CL. The PTEN/MMAC1 tumor suppressor phosphatase functions as a negative regulator of the phosphoinositide 3-kinase/Akt pathway. Proceedings of the National Academy of Sciences of the United States of America. 1998; 95:15587–91. [PubMed: 9861013]
10. PUC J, Keniry M, Li H, PANDITA T, CHOUDHURY A, MEMEO L, et al. Lack of PTEN sequesters CHK1 and initiates genetic instability. Cancer Cell. 2005; 7:193–204. [PubMed: 15710331]
11. Mendes-Pereira AM, Martin SA, Brough R, McCarthy A, Taylor JR, Kim J-S, et al. Synthetic lethal targeting of PTEN mutant cells with PARP inhibitors. EMBO Mol Med. 2009; 1:315–22. [PubMed: 20049735]
12. Bryant HE, Schultz N, Thomas HD, Parker KM, Flower D, Lopez E, et al. Specific killing of BRCA2-deficient tumours with inhibitors of poly(ADP-ribose) polymerase. Nature. 2005; 434:913–7. [PubMed: 15829966]
13. Chen Z, Trotman LC, Shaffer D, Lin H-K, Dotan ZA, Niki M, et al. Crucial role of p53-dependent cellular senescence in suppression of Pten-deficient tumorigenesis. Nat Cell Biol. 2005; 436:725–30.
14. Marte BM, Downward J. PKB/Akt: connecting phosphoinositide 3-kinase to cell survival and beyond. Trends in Biochemical Sciences. 1997; 22:355–8. [PubMed: 9301337]
15. Hers I, Vincent EE, Tavaré JM. Akt signalling in health and disease. Cellular Signalling. Elsevier Inc. 2011; 23:1515–27.
16. Tapodi A. Pivotal Role of Akt Activation in Mitochondrial Protection and Cell Survival by Poly(ADP-ribose)polymerase-1 Inhibition in Oxidative Stress. Journal of Biological Chemistry. 2005; 280:35767–75. [PubMed: 16115861]
17. Juvekar A, Burga LN, Hu H, Lunsford EP, Ibrahim YH, Balmana J, et al. Combining a PI3K Inhibitor with a PARP Inhibitor Provides an Effective Therapy for BRCA1-Related Breast Cancer. Cancer Discovery. 2012; 2:1048–63. [PubMed: 22915751]
18. Schnell CR, Stauffer F, Allegrini PR, O'Reilly T, McSheehy PMJ, Dartois C, et al. Effects of the Dual Phosphatidylinositol 3-Kinase/Mammalian Target of Rapamycin Inhibitor NVP-BEZ235 on the Tumor Vasculature: Implications for Clinical Imaging. Cancer Res. 2008; 68:6598–607. [PubMed: 18701483]
19. Yuan TL, Choi HS, Matsui A, Benes C, Lifshits E, Luo J, et al. Class 1A PI3K regulates vessel integrity during development and tumorigenesis. Proceedings of the National Academy of Sciences. 2008; 105:9739–44.
20. Lunardi A, Ala U, Epping MT, Salmena L, Clohessy JG, Webster KA, et al. Nature Publishing Group. Nature Publishing Group. 2013; 45:747–55. ng.2650.
21. Trotman LC, Niki M, Dotan ZA, Koutcher JA, Di Cristofano A, Xiao A, et al. Pten Dose Dictates Cancer Progression in the Prostate. Plos Biol. 2003; 1:e9. [PubMed: 14551907]
22. Nastiuk KL, Liu H, Hamamura M, Muftuler LT, Nalcioglu O, Krolewski JJ. In vivo MRI volumetric measurement of prostate regression and growth in mice. BMC Urol. 2007; 7:12. [PubMed: 17650332]
23. Park J-H, Walls JE, Galvez JJ, Kim M, Abate-Shen C, Shen MM, et al. Prostatic Intraepithelial Neoplasia in Genetically Engineered Mice. The American Journal of Pathology. American Society for Investigative Pathology. 2010; 161:727–35.

SIGNIFICANCE

The paucity of therapeutic options in advanced CaP display an urgent need for the pre-clinical assessment of novel therapeutic strategies. We identified differential therapeutic vulnerabilities that emerge upon loss of both PTEN and p53 and observed that combined inhibition of PARP and PI3K provides increased efficacy in hormone insensitive advanced CaP.

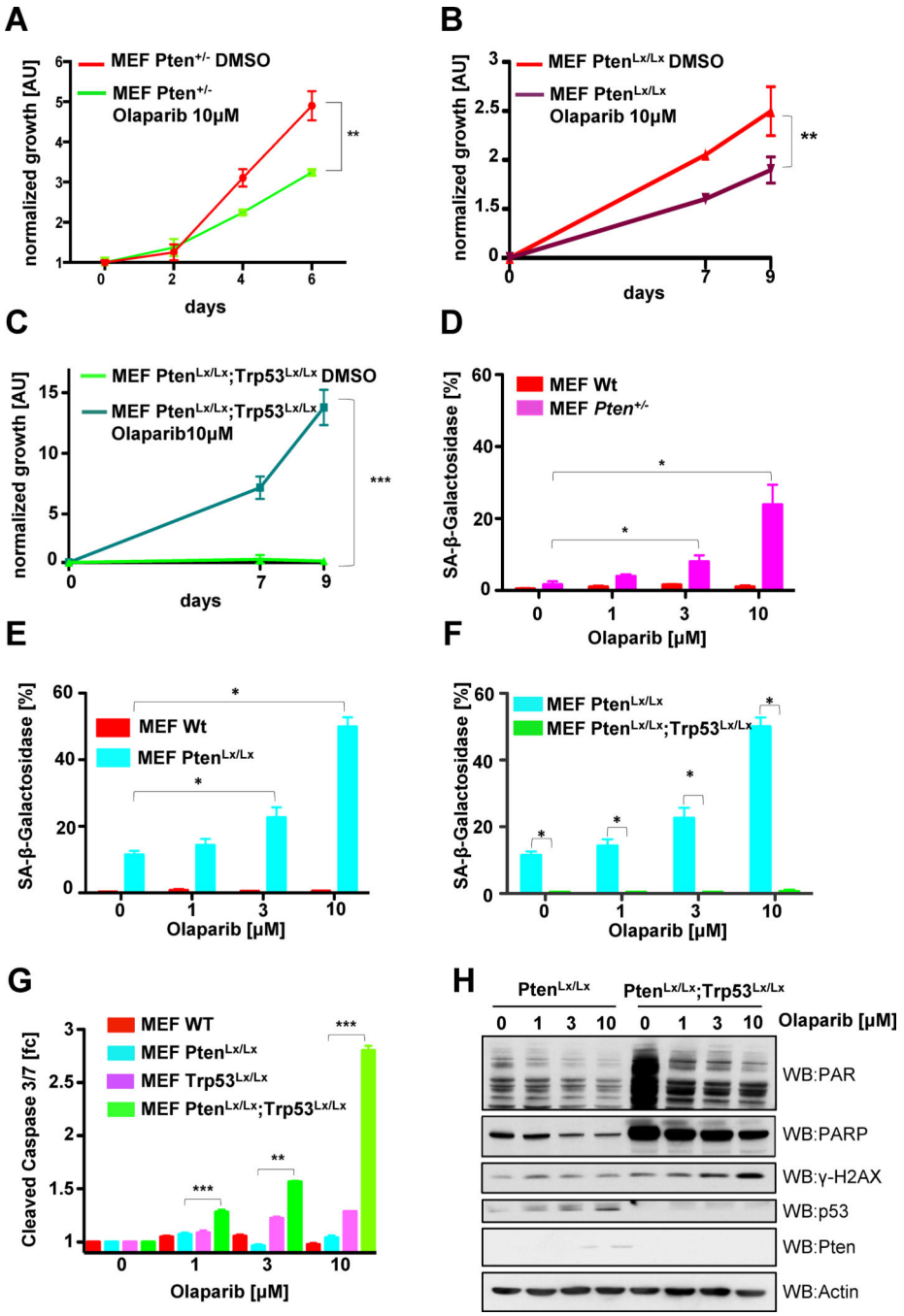

Figure 1. Common genetic alterations in prostate cancer morph senescence into apoptosis in response to PARP inhibition

Growth of (**A**) *Pten*$^{+/-}$ (**B**) *Pten*$^{Lx/Lx}$ and (**C**) *Pten*$^{Lx/Lx}$*;Trp53*$^{Lx/Lx}$ MEFs in the presence of 10 μM Olaparib (**p<0.0032; ***p<0.0001). (**D**)Quantification of SA-β-gal positivity in *Pten*$^{+/-}$ and (**E**) *Pten*$^{Lx/Lx}$ MEF upon increasing doses of Olaparib at Day 4 (*p<0.05). (**F**)Quantification of SA-β-gal positivity in *Pten*$^{Lx/Lx}$ compared to *Pten*$^{Lx/Lx}$*;Trp53*$^{Lx/Lx}$ MEFs upon increasing doses of Olaparib at Day 4 (*p<0.05). (**G**) Quantification of Caspase 3/7 activity after treatment with 10uM Olaparib for 48hrs (**p<0.01; ***p<0.001). (**H**)

Western Blot analysis of *Pten*$^{Lx/Lx}$ and *Pten*$^{Lx/Lx}$;*Trp53*$^{Lx/Lx}$ MEFs after 3 days of Olaparib treatment.

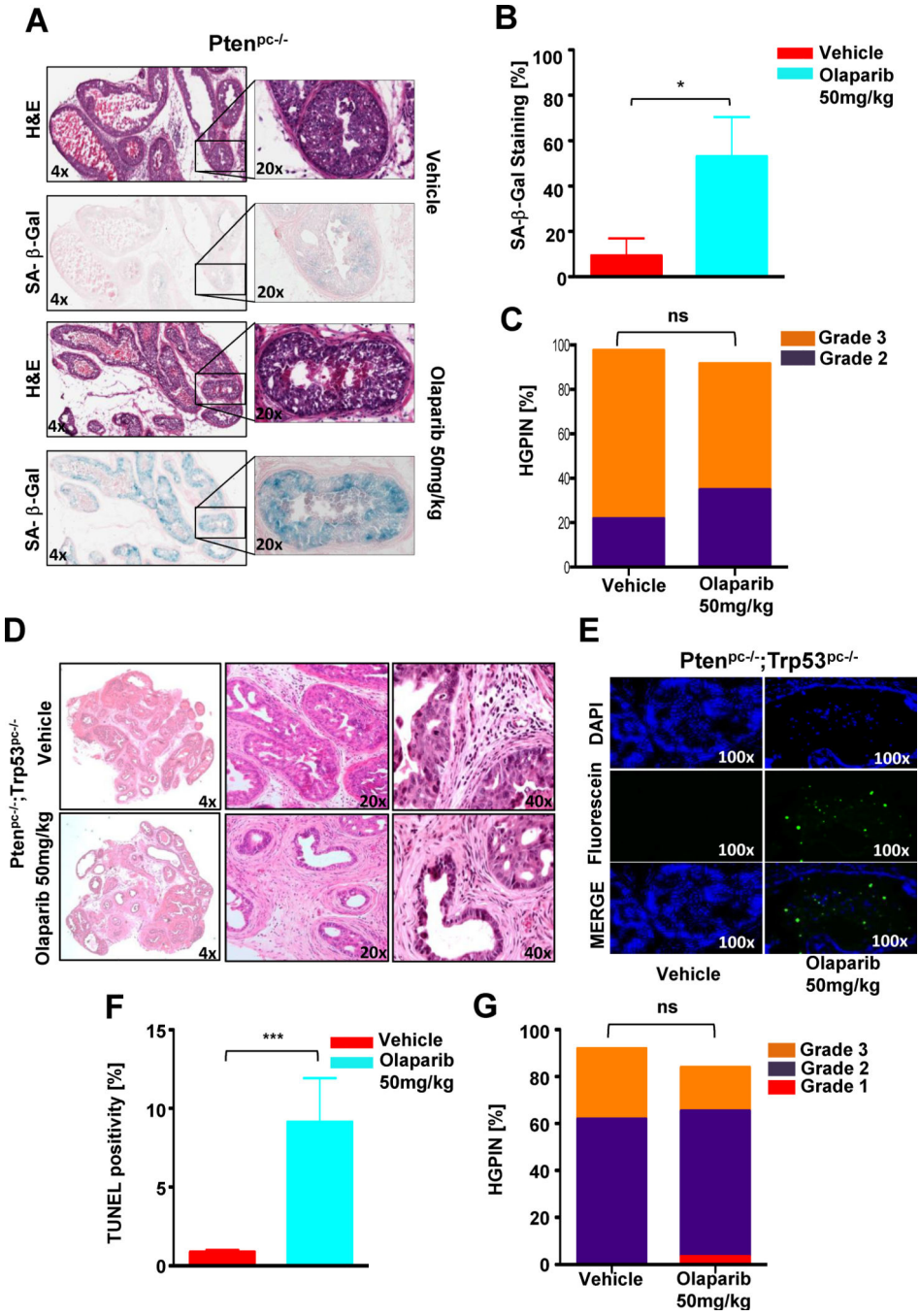

Figure 2. PARP inhibition induces a differential response *in vivo* with a modest effect on overall tumor response

(**A**) SA-β-gal staining in prostates of 8 week old *Pten*$^{pc-/-}$ mice upon Olaparib (n=3) or vehicle (n=3) treatment for 2 weeks. (**B**) Quantification of SA-β-gal positivity from (A) (*p=0.0419). (**C**) Histopathological analysis of HGPIN status from (A). (**D**) H&E staining of DLP tumors from 4 month old *Pten*$^{pc-/-}$;*Trp53*$^{pc-/-}$ mice upon Olaparib (n=3) or vehicle (n=3) treatment for 1 week. (**E**) TUNEL staining to visualize apoptosis induction in (D) and

(**F**) its quantification (***p=0.0006). (**G**) Histopathological analysis of HGPIN status from (D).

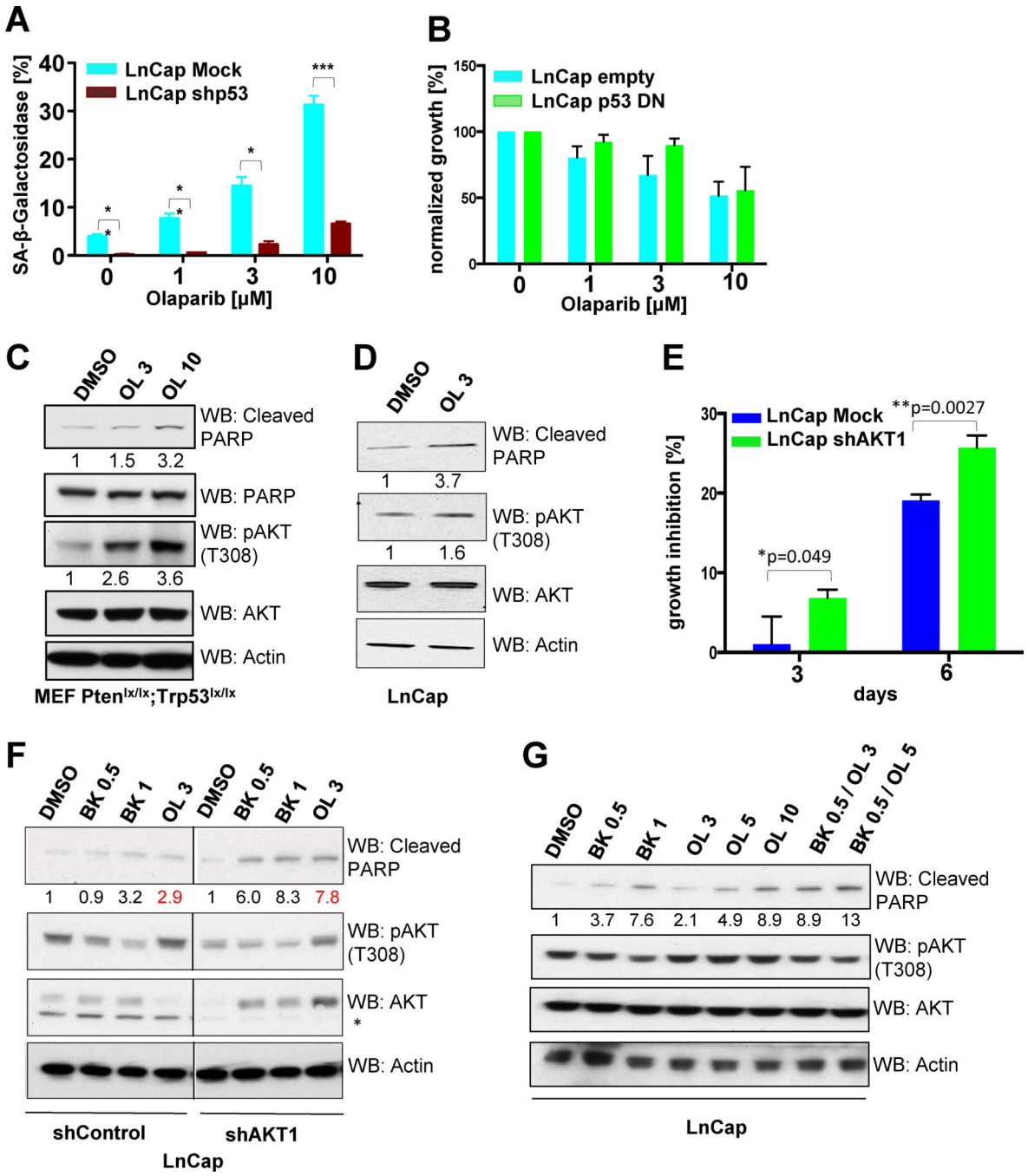

Figure 3. Hyperactivation of the PI3K-Akt pathway impacts sensitivity towards Olaparib

(**A**) Quantification of SA-β-gal positivity towards increasing doses of Olaparib after 4 days in LnCap cells upon stable P53 knockdown (n=4; *p=0.01; **p<0.008; ***p=0.0006). (**B**) Quantification of growth inhibition towards increasing doses of Olaparib after 3 days in LnCap cells overexpressing dominant negative (DN) p53 (n=2). (**C**) Western Blot analysis of Akt activation in *Pten*$^{Lx/Lx}$*;Trp53*$^{Lx/Lx}$ MEFs after 24h and (**D**) LnCap cells after 72h cells of Olaparib treatment. (**E**) Quantification of growth inhibition upon Olaparib treatment (5uM) after Akt1 knockdown in LnCap cells. (**F**) Western Blot analysis of apoptosis

induction in LnCap after Akt1 knockdown upon Olaparib treatment for 72h. (**G**) Western Blot analysis of apoptosis induction in LnCap upon Olaparib, BKM-120 or combination treatment for 72h.
OL=Olaparib; BK=BKM-120

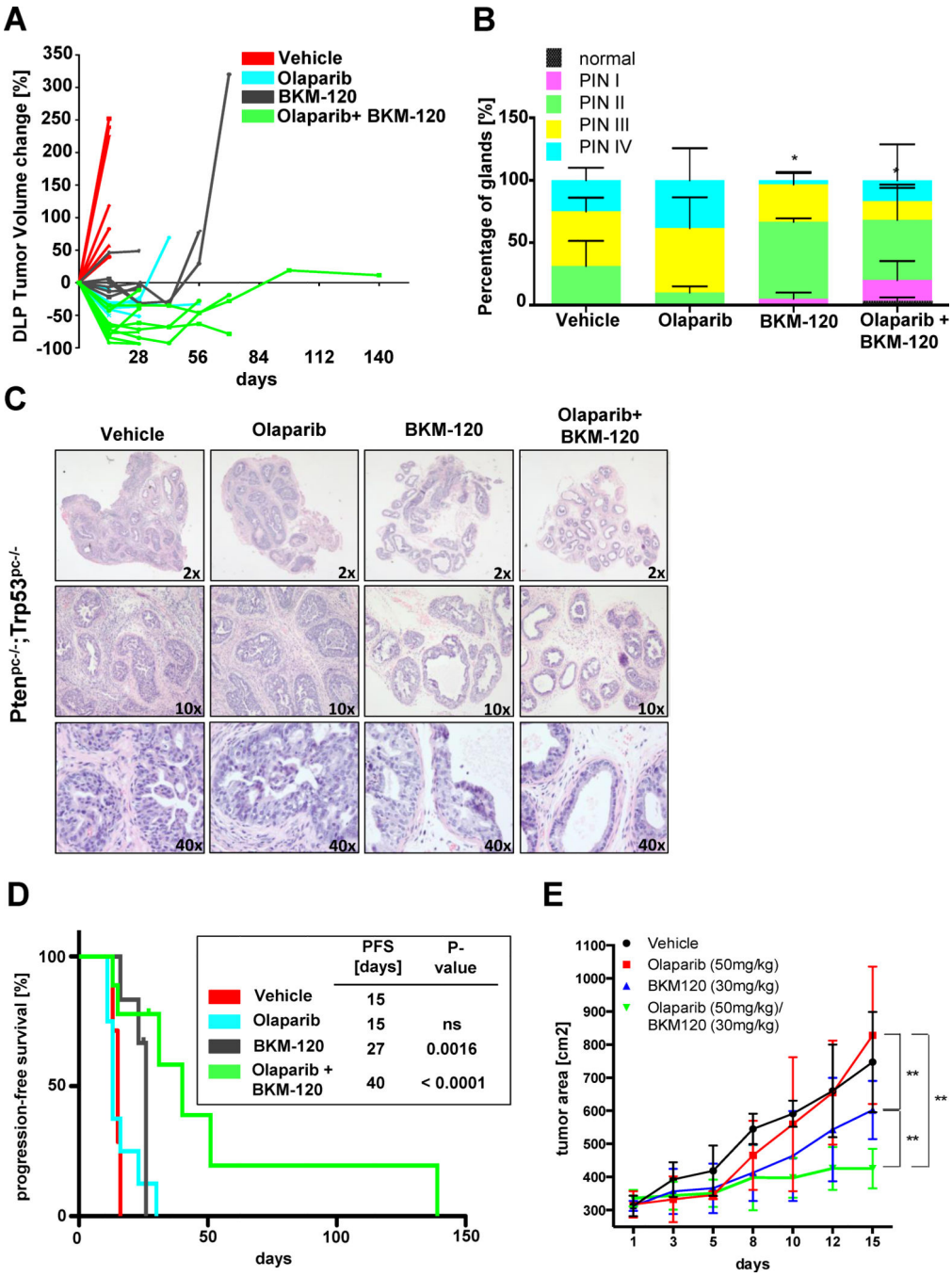

Figure 4. Combination of PARP and PI3K inhibitors as a novel therapeutic approach

(**A**) DLP tumor volume change of *Pten*$^{pc-/-}$;*Trp53*$^{pc-/-}$ mice upon vehicle (n=7), Olaparib (n=8), BKM-120 (n=6) or combination (n=9) treatment. (**B**) Histopathological analysis of HGPIN status from vehicle (n=3, 1 and 4 weeks pooled), Olaparib (n=3), BKM-120 (n=3) or combination (n=3) treatment for 4 weeks (*p<0.03). (**C**) H&E staining from (A). (**D**) Progression free survival of *Pten*$^{pc-/-}$;*Trp53*$^{pc-/-}$ mice upon vehicle (n=7), Olaparib (n=8), BKM-120 (n=6) or combination (n=9) treatment. (**E**) Tumor growth of PC3 xenografts upon

vehicle (n=5), Olaparib (n=5), BKM-120 (n=4) or combination (n=5) (**p<0.009) treatment. Olaparib=50mg/kg; BKM-120=30mg/kg